Supplementary material for

"Non-centrosymmetric Weyl Semimetal State and Strain Effect in the Twisted-brick Phase Transition Metal Monochalcogenides"

Jia-Fang Wu,[1] Sha-Sha Ke,[1] Yong Guo,[2] Huai-Wu Zhang,[1] and Hai-Feng Lü[1,2,*]

[1]*School of Physics and State Key Laboratory of Electronic Thin Films and Integrated Devices, University of Electronic Science and Technology of China, Chengdu 610054, China*

[2]*Department of Physics and State Key Laboratory of Low-Dimensional Quantum Physics, Tsinghua University, Beijing 100084, China*

1. The electronic structure and its phonon dispersion in WTe.

The bands near the Fermi level are mainly composed of W orbitals and a small proportion of Te orbitals for WTe, as shown in Fig. 1S (a). And further considering the contact points between the valence band (VB) and conduction band (CB) of WTe in the whole Brillouin zone (BZ) without and with spin-orbit coupling (SOC), the results show that there is no touching point, exhibiting a compensated semimetal state. The phonon dispersion bands of WTe have no negative frequencies, as shown in Fig. 1S (b), which indicates that the optimized WTe structures are dynamically stable.

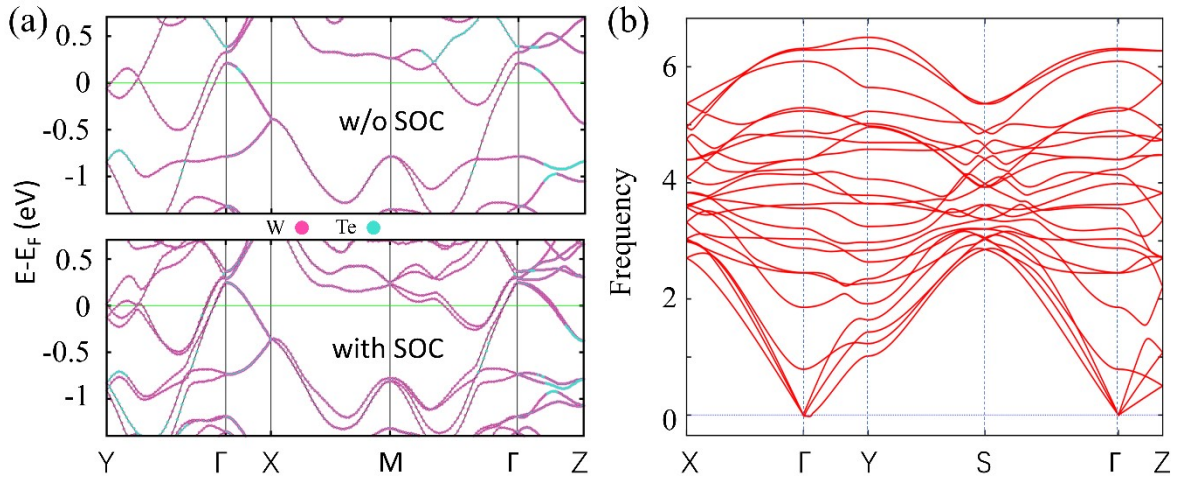

Fig. 1S (a) Bulk band structure of fully relaxed WTe without SOC and with SOC. The bands of WTe system have a direct gap along the high symmetry line. The pink and turquoise dots represent the total orbit resolved of the W atom and the Te atom. (b) Phonon dispersion curve for the twisted-brick phase of WTe.

2. The electronic band structure of MoTe using the HSE06 functional without SOC.

The nodal loop states are double-checked by the HSE06 functional in the absence of SOC. The crossing points at -0.72 eV along the Y-Γ high symmetry line maintain in the HSE06 band structure, as shown in Fig. 2S. The results show that the overall form of band structures of the MoTe system along the high symmetry line is the same in PBE and HSE06 functional calculations.

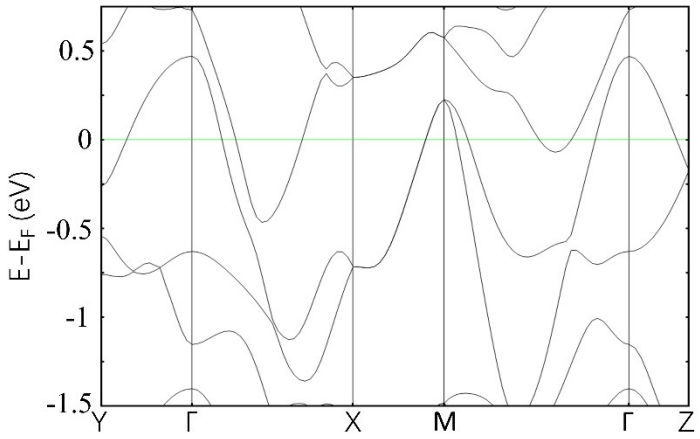

Fig. 2S The electronic band structures along high-symmetry directions of the BZ of the twisted-brick phase MoTe predicted using the HSE06 functional without SOC.

3. The band-inversion phenomenon of MoTe in the absence of SOC.

The bands near the Fermi level are mainly composed of Mo-d orbitals. By resolving the different *d* orbitals, a clear indication of the strong mixing between the five orbitals near the Fermi level is as shown in Fig. 3S (a). One can see that the two crossing bands along Y-Γ have a nontrivial band inversion between the Mo-$d_{x^2-y^2}$ orbital and Mo-d_{xz} orbital, as shown in Fig. 3S (b) (shaded in grey).

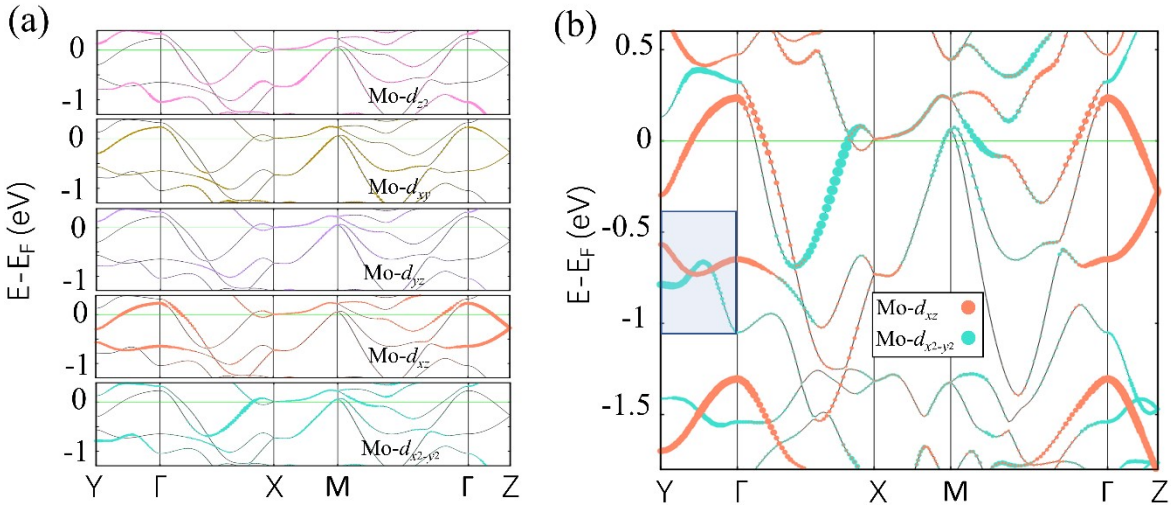

Fig. 3S Orbital-resolved bands without SOC for MoTe near the Fermi level. Different colored circles represent different orbital projections of Mo atoms. The size of the circles represents the weight of the orbital projection.

4. Thermal stability and dynamic stability for MoTe under uniaxial strain.

The time evolution of temperature and total energy per formula unit cell in AIMD calculations for MoTe under uniaxial strain (ε_z = +4%, +8%) are shown in Fig. 4S (c-f). A stable thermal long-timescale fluctuation around average values up to 12 *ps* demonstrates the thermal stability of their structures at room temperature.

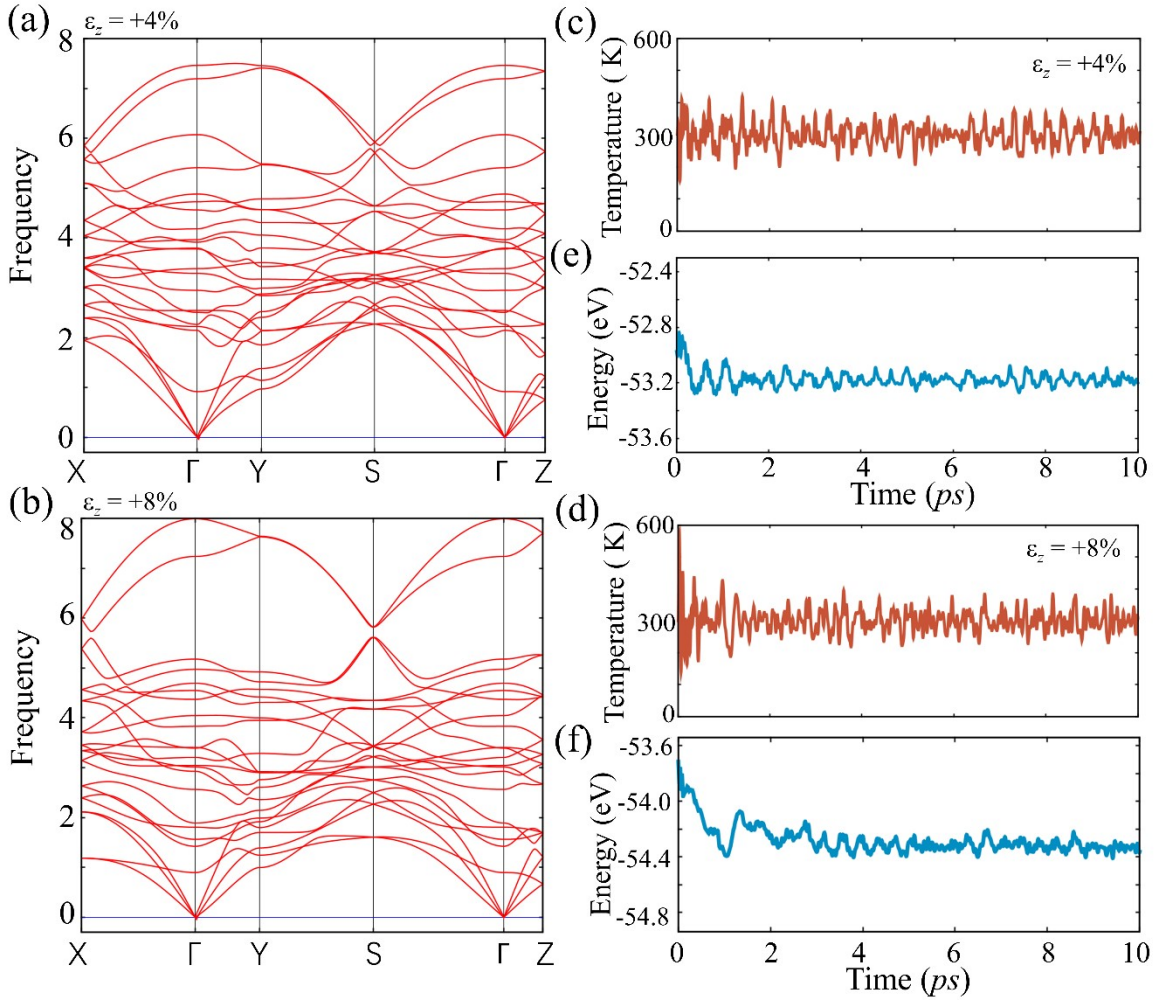

Fig. 4S The phonon dispersions for MoTe under strain (a) ε_z = +4% and (b) ε_z = +8%. The temperature and total energy per unit cell of simulation time in AIMD calculations for WTeS under (c, e) ε_z = +4% and (d, f) ε_z = +8% strain.

5. The effects of uniaxial strain in MoTe with SOC.

Fig. 5S (a) shows the evolution of the average energy of Weyl points (WPs) and the *k* space maximal distance (Δk) between a pair of WPs as a non-monotonous function of uniaxial strain, respectively. Our calculation shows that the Δk and average energy both first increase and then decrease as the strain varies from compressive to tensile. It is just that the average energy of WPs increases rapidly at tensile strain. The Δk is of the order of magnitude of 0.1 $Å^{-1}$ and reaches the peak at around 1.08 $Å^{-1}$ and 0.55 $Å^{-1}$ under compressive 6% and tensile 10% strains, respectively. Very interestingly, we find tensile uniaxial strain also increases the separation between the nearest WPs. A further change of the strain makes one of the two WPs hit the mirror plane M_{yz} (or $k_x = 0.5 \times 2\pi/c$ planes, where it is annihilated with its mirror-symmetrical point of opposite chirality, and thus reduced WPs are out of the $k_x = 0$, $0.5 \times 2\pi/c$ planes. Additionally, since under time reversal a WP at (k_x, k_y, k_z) is converted into a Weyl node at ($-k_x$, $-k_y$, $-k_z$) with the same chirality. Therefore, the total number of WPs is annihilated with a multiple of four. This situation is illustrated in Fig. 5S (b). Therefore, we

can conclude that the uniaxial strain effect can tune the WPs of MoTe to the new location and then generate or annihilate WPs.

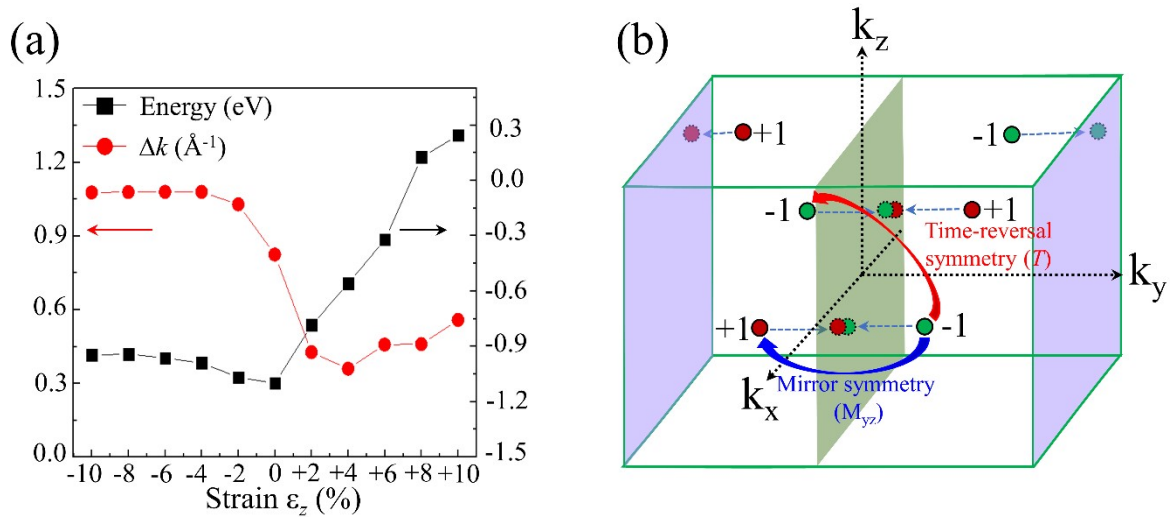

Fig. 5S (a) The changes of the average energy of Weyl points and maximal separation (Δk) between Weyl points under uniaxial strain. (b) Schematic illustration of the effect of uniaxial tensile strain along the *z* direction.